

ONSET OF CAVITY DEFORMATION UPON SUBSONIC MOTION OF A PROJECTILE IN A FLUID COMPLEX PLASMA

D. I. Zhukhovitskii,^{1,*} A. V. Ivlev,² V. E. Fortov,¹ and G. E. Morfill²

¹*Joint Institute of High Temperatures, Russian Academy of Sciences, Izhorskaya 13, Bd. 2, 125412 Moscow, Russia*

²*Max-Planck-Institut für extraterrestrische Physik, Giessenbachstrasse, 85748 Garching, Germany*

(Dated: August 29, 2018)

We study the deformation of a cavity around a large projectile moving with subsonic velocity in the cloud of small dust particles. To solve this problem, we employ the Navier–Stokes equation for a compressible fluid with due regard for friction between dust particles and atoms of neutral gas. The solutions shows that due to friction, the pressure of a dust cloud at the surface of a cavity around the projectile can become negative, which entails the emergence of a considerable asymmetry of the cavity, i.e., the cavity deformation. Corresponding threshold velocity is calculated, which is found to decrease with increasing cavity size. Measurement of such velocity makes it possible to estimate the static pressure inside the dust cloud.

PACS numbers: 52.27.Lw, 83.10.Rs, 82.70.Dd

I. INTRODUCTION

Complex (dusty) plasma is a low-temperature plasma including microparticles. Due to electron absorption, particles acquire a considerable electric charge. Thus, a strongly coupled Coulomb system is formed [1–9]. Such plasma represents a natural system which makes it possible to observe various collective phenomena at the level of individual particles. In experimental setups, complex plasmas are usually studied in gas discharges at low pressures, e.g., in radio frequency (RF) discharges. A large homogeneous bulk of complex plasma, which almost fills the entire discharge volume, can be observed under microgravity conditions either in parabolic flights [10–14] or onboard the International Space Station (ISS) [10, 15–19].

In recent studies, attention was focused on tracer particles or projectiles moving through a cloud of complex plasma. Such projectiles are generated using controlled mechanisms of acceleration [11, 20], or they can appear sporadically [19, 21]. Projectiles moving with supersonic velocity lead to the formation of extended Mach cones; subsonic (slow) ones produce localized disturbances of surrounding particles. In Ref. 22, it was suggested that the latter regime, realized when a relatively large subsonic projectile moves in a dense cloud of smaller particles, can be well approximated by a flow of an incompressible fluid. In the framework of the same hydrodynamic approximation, it was demonstrated that, along with the regular neutral gas drag, there is an additional force exerted on the projectile due to friction between neutral atoms and the particle fluid [23].

In this study, we try to estimate the deformation threshold for an (initially spherical) cavity around a subsonic projectile. This deformation emerges abruptly as

the projectile velocity increases, as it is seen in snapshots given in [11, 22]. To solve this problem, we employ the Navier–Stokes equation for a compressible fluid taking into account friction between dust particles and atoms of neutral gas. We do not treat the deformation self-consistently. Instead, we imply that the projectile velocity is below the threshold value, so that a regular flow around a spherical cavity with no stall can be treated. The solutions shows that due to friction, the pressure of a dust cloud at the boundary of the cavity behind the projectile can become negative, which entails the formation of a microscopic void free from dust particles, i.e., the cavity deformation. This occurs at some threshold velocity which decreases with increasing cavity size. Measurement of such velocity would make it possible to estimate the static pressure inside the dust cloud.

The paper is organized as follows. In Sec. II, we solve the non-stationary Navier–Stokes equation for an incompressible particle fluid. In Sec. III, the gas dynamics problem is solved and the corrections for fluid compressibility to the velocity and pressure fields are calculated. Calculation results are compared with available experimental data in Sec. IV and the results of this study are summarized in Sec. V.

II. INCOMPRESSIBLE FLUID APPROXIMATION

Consider an irrotational flow of incompressible particle fluid formed by the dust crystal melted around a projectile moving with the velocity $\mathbf{u}(t)$ relative to the dust, where t is the time. The parameter of interaction between dust particles is large due to their low kinetic energy at room temperature. The corresponding parameter for the interaction between the projectile and dust particles can be defined as the ratio of characteristic Coulomb energy to the kinetic energy of a dust particle,

* dmr@ihed.ras.ru

$\beta_{dp} = 2Z_p Z_d e^2 / \lambda M_d u^2$ (where Z_p and Z_d are the charges of the projectile and dust particle, respectively, in units of the electron charge e , $\lambda \simeq 6 \times 10^{-3}$ cm is the plasma (ion) screening length, and M_d is the dust particle mass). Under typical conditions, this parameter is great, $\beta_{dp} \sim 100$ [22]. In such a strongly coupled system, each particle (including the projectile) finds itself in the center of the spherically symmetric Wigner–Seitz cell. Since each cell is electrically neutral, the interaction of particles can be effectively reduced to that of cell surfaces, which can be modeled by hard spheres. This applies to the surface of a cell around the projectile as well. This approach is valid until the cavity deformation occurs; however, we will confine ourselves to the treatment of spherically symmetric cavities below the deformation threshold. We denote the radius of a cavity around the projectile by R .

The Navier–Stokes equation describing the velocity field $\mathbf{v}(\mathbf{r}, t)$ in the reference frame of the projectile has the form

$$\frac{\partial \mathbf{v}}{\partial t} + (\mathbf{v} \cdot \nabla) \mathbf{v} + \nu(\mathbf{v} + \mathbf{u}) = -\frac{\nabla p}{\rho}, \quad (1)$$

where $\rho = M_d n_d$ is the mass density of dust fluid (assumed in this section to be constant), with M_d and n_d being, respectively, the mass and number density of dust particles of the radius a_d . Furthermore, $p(t, \mathbf{r})$ is the dust pressure field, $\nu = (8\sqrt{2\pi}/3)\delta m_n n_n v_{T_n} a_d^2 / M_d$ is the friction coefficient with $\delta \simeq 1.4$ being the accommodation coefficient [6], and m_n , n_n , T_n , and $v_{T_n} = (T_n/m_n)^{1/2}$ are the mass, number density, temperature, and thermal velocity of neutral gas molecules, respectively. Equation (1) assumes also that far from the projectile, dust particles are quiescent relative to neutral gas. It was shown in [22] that the approximation of nonviscous flow results in a fairly good description of trajectories of individual dust particles; the estimate of the viscosity term for the dust particle fluid is indicative of the fact that in most cases, it is small [23]. This allowed us to omit it in Eq. (1) and to confine ourselves to the nonviscous approximation.

For an incompressible fluid, the continuity equation is reduced to

$$\nabla \cdot \mathbf{v} = 0. \quad (2)$$

The boundary conditions for (1) and (2) are $(\mathbf{v} \cdot \mathbf{n})|_{r=R} = 0$, where $\mathbf{n} = \mathbf{r}/r$, and $\mathbf{v} = -\mathbf{u}$ at $r = \infty$. For an irrotational flow ($\nabla \times \mathbf{v} = 0$), we substitute $\mathbf{v} = \nabla \varphi - \mathbf{u}$ in Eq. (2) to obtain the equation

$$\nabla^2 \varphi = 0, \quad \varphi(t, \infty) = 0, \quad \frac{\partial \varphi}{\partial \mathbf{n}} \Big|_{r=R} = 0, \quad (3)$$

which has the solution [24]

$$\varphi(\mathbf{r}) = -\frac{R^3}{2r^2} \mathbf{u} \cdot \mathbf{n} \quad (4)$$

or

$$\mathbf{v}(\mathbf{r}) = -\frac{R^3}{2r^3} [\mathbf{u} - 3\mathbf{n}(\mathbf{n} \cdot \mathbf{u})] - \mathbf{u}. \quad (5)$$

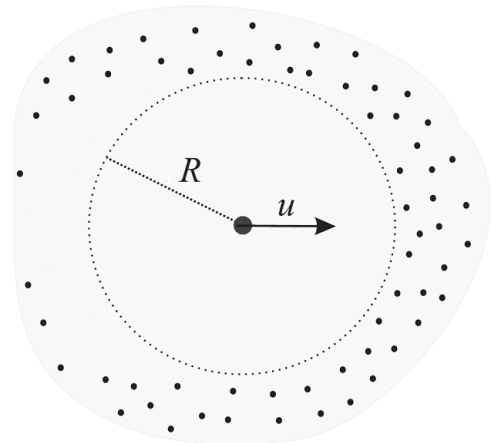


FIG. 1. Deformation of a cavity behind moving projectile (large bullet in the center) moving with the velocity u through the dust crystal (small bullets around) in a carrier gas. The projectile is surrounded by deformed cavity with initial radius R .

The pressure field $p(\mathbf{r})$ can then be found by substituting velocity (5) in Eq. (1). This yields the following pressure distribution at the spherical surface of a cavity ($r = R$),

$$p = p_{st} + \frac{\rho \nu R}{2} \mathbf{u} \cdot \mathbf{n} + \frac{\rho u^2}{8} \left[9 \frac{(\mathbf{u} \cdot \mathbf{n})^2}{u^2} - 5 \right] + \frac{\rho R}{2} \dot{\mathbf{u}} \cdot \mathbf{n}, \quad (6)$$

where $p_{st} = \text{const} > 0$ is the static pressure of dust at $r = \infty$.

Consider the deformation of a cavity around a projectile propagating in the dust crystal (Fig. 1). Here, we will neglect finite fluid compressibility – corresponding corrections are discussed in Sec. III. Deformation can be caused solely by the formation of a void in the stream of dust fluid because the interaction parameter β_{dp} is large. Since no evidence for an appreciable attraction between dust particles has been reported in the literature, we model the cloud of dust particles by a system of hard spheres. In such a system, a cavity can be deformed by void formation if the condition $p \leq 0$ is satisfied over some area around a cavity. This condition corresponds to cavitation in a metastable fluid and to stall in gas dynamics.

Let us first consider the case $\dot{u} = 0$. According to Eq. (6), friction between dust particles and neutral gas gives rise to a pressure increase in front of the projectile and a decrease behind it, so that $p(\mathbf{r})$ reaches a maximum at the “front pole” (where $\mathbf{u} \cdot \mathbf{n} = u$). By introducing the cosine of the polar angle, $\cos \theta = \mathbf{u} \cdot \mathbf{n} / u \equiv \xi$, we readily derive

$$\frac{\partial p}{\partial \xi} = \frac{9}{4} \rho u^2 (\xi - \xi_{cr}), \quad (7)$$

where $\xi_{cr} = -2\nu R / 9u$. If $|\xi_{cr}| > 1$ then the pressure reaches a minimum at the “rear pole” ($\xi = -1$), where

$p_{\min} = p_{\text{st}} - \rho u^2(9|\xi_{\text{cr}}|/2 - 1)/2$. This corresponds to the low-velocity regime $u < 2\nu R/9$, when the minimum pressure decreases (approximately) linearly both with u and R . The cavity deformation threshold is defined by the condition $p_{\min} = 0$ and is reached easier for larger projectiles, at the critical velocity $u_{\text{cr}} \simeq 2p_{\text{st}}/(\rho\nu R)$ [here we assume $p_{\text{st}} \lesssim \rho(\nu R)^2/8$]. Note that in the high-velocity regime $u > 2\nu R/9$ the pressure minimum is shifted to a certain latitude in the rear hemisphere, approaching the “equator” ($\xi = 0$) asymptotically. In this case friction plays a minor role and the critical velocity is $u_{\text{cr}} \simeq \sqrt{8p_{\text{st}}/5\rho}$.

Note that for arbitrary acceleration (assuming $\dot{\mathbf{u}}\|\mathbf{u}$), one can introduce the effective damping rate $\nu_{\text{eff}} = \nu + \dot{u}/u$ which can have either sign, so that the critical cosine ξ_{cr} can have either sign as well. Thus, if a projectile experiences sufficiently strong deceleration ($|\dot{u}|/u > \nu$), the cavity can also be deformed at the front hemisphere.

The critical velocity u_{cr} calculated above defines the emergence of a point or circle of zero pressure on the cavity surface depending on the value of ξ_{cr} . It is well-known in gas dynamics that the existence of small local regions of negative pressure would not lead to a significant deformation of flow lines and, therefore, to a stall. Instead, stall emergence requires an extended region of negative pressure that covers a significant part of “rear hemisphere”. There does not seem to be any criterion that would tell us how large the negative region should be to initiate a stall. Nevertheless, one can hope that the velocity u_{cr} derived above provides a reasonable lower bound estimate for the cavity deformation onset. Strictly speaking, the theory discussed above is not applicable for the case $u > u_{\text{cr}}$ because a streamlined cavity is already deformed. At the same time below the stall threshold, this deformation is small, i.e., the cavity is still almost spherical. Therefore, one could extend the analysis to the region of the velocities higher than the critical one and, respectively, to the region of negative pressure larger than a point or a circle on the cavity surface. In the next Section, obtained results are generalized to the case of the finite compressibility of a fluid.

III. FLOW WITH FINITE COMPRESSIBILITY

In this Section, we will estimate the effect of finite compressibility of the dust cloud on the velocity and pressure fields. Here, we will treat a steady ($\dot{\mathbf{u}} = 0$) and irrotational ($\nabla \times \mathbf{v} = 0$) flow, so that the fluid density is a function solely of the radius-vector: $\rho = \rho(\mathbf{r})$. Since $\nabla \times \mathbf{v} = 0$ and $\nabla p = c^2 \nabla \rho$, where $c = \sqrt{(\partial p / \partial \rho)_T}$ is the sound velocity, we can rewrite Eq. (1) in the form

$$(\mathbf{v} \cdot \nabla) \mathbf{v} + \nu(\mathbf{v} + \mathbf{u}) = -\frac{c^2}{\rho} \nabla \rho. \quad (8)$$

In this case, the continuity equation includes the fluid density,

$$\nabla \cdot \mathbf{v} + \mathbf{v} \cdot \frac{\nabla \rho}{\rho} = 0. \quad (9)$$

Here, c is assumed to be constant independent of the local velocity and plasma state parameters. We substitute $\nabla \rho / \rho = -(1/c^2)(\mathbf{v} \cdot \nabla) \mathbf{v} - (\nu/c^2)(\mathbf{v} + \mathbf{u})$ from (8) in (9) to derive

$$\nabla \cdot \mathbf{v} = \frac{1}{c^2} \mathbf{v} \cdot (\mathbf{v} \cdot \nabla) \mathbf{v} + \frac{\nu}{c^2} (v^2 + \mathbf{u} \cdot \mathbf{v}). \quad (10)$$

We will search for the solution of Eq. (10) in the form $\mathbf{v} = \mathbf{v}_0 + \mathbf{v}_1$, where $\mathbf{v}_0(\mathbf{r})$ is the solution of incompressible problem (for $\rho = \rho_0 = \text{const}$, i.e., for $c \rightarrow \infty$) given by Eq. (5), the respective pressure distribution $p_0(\mathbf{r})$ is presented by Eq. (6) (for $\dot{u} = 0$). Obviously, $\nabla \cdot \mathbf{v}_0 = 0$. We assume that $|\mathbf{v}_1| \ll |\mathbf{v}_0|$ and retain solely zeroth-order terms on the rhs of (10) to obtain

$$\nabla \cdot \mathbf{v}_1 = \frac{1}{2c^2} \mathbf{v}_0 \cdot \nabla v_0^2 + \frac{\nu}{c^2} (v_0^2 + \mathbf{u} \cdot \mathbf{v}_0). \quad (11)$$

Here, we took into account that $\nabla \times \mathbf{v}_0 = 0$ and hence $(\mathbf{v}_0 \cdot \nabla) \mathbf{v}_0 = \nabla v_0^2 / 2$. Since $|\mathbf{v}_0| \sim u$, $|\nabla| \sim 1/R$, and $(u/c)^2$ is small for subsonic motion, the estimate $|\mathbf{v}_1| \sim (u^2/c^2) \max\{u, \nu R\}$ following from (11) justifies our assumption. It is seen from this estimate that both sides of Eq. (11) are of the order $(u/c)^2$, and terms other than zeroth-order ones would lead to higher-order terms in this parameter. Obviously, $|\mathbf{v}_1| \rightarrow 0$ at $c \rightarrow \infty$.

We introduce the scaled coordinate $x = r/R$ and the dimensionless potential $\tilde{\varphi}_1$ defined by the relation $\mathbf{v}_1 = (u^3/c^2) \nabla \tilde{\varphi}_1$ (in so doing, the condition $\nabla \times \mathbf{v}_1 = 0$ is satisfied) to rewrite (11) in the dimensionless form

$$\begin{aligned} \nabla^2 \tilde{\varphi}_1 = & \frac{\kappa}{2x^6} P_0(\xi) + \left(\frac{36}{5x^7} - \frac{9}{2x^{10}} \right) P_1(\xi) \\ & - \kappa \left(\frac{1}{x^3} - \frac{1}{2x^6} \right) P_2(\xi) \\ & - \left(\frac{6}{x^4} - \frac{24}{5x^7} + \frac{3}{2x^{10}} \right) P_3(\xi), \end{aligned} \quad (12)$$

where $P_l(\xi)$ are the Legendre polynomials and $\kappa = \nu R/u$. Here and in what follows, differentiation with respect to scaled coordinates is assumed. The boundary conditions for Eq. (12) follow from the conditions $\mathbf{v}_1(\infty) = 0$ and $\mathbf{n} \cdot \mathbf{v}_1|_{r=R} = 0$, i.e.,

$$\tilde{\varphi}_1(\infty) = 0, \quad \left. \frac{d\tilde{\varphi}_1}{dx} \right|_{x=1} = 0. \quad (13)$$

Solution of Eq. (12) is derived in Appendix A. The resulting finite-compressibility corrections to the potential and velocity at the cavity surface follow from (A6):

$$\begin{aligned} \tilde{\varphi}_1|_{x=1} = & \frac{81}{176} \xi^3 + \frac{\kappa}{2} \left(\frac{1}{4} \xi^2 - \frac{1}{3} \right) - \frac{551}{880}, \\ \mathbf{v}_1|_{x=1} = & \frac{u^2}{c^2} \left(\frac{243}{176} \xi^2 + \frac{\kappa}{4} \xi - \frac{551}{880} \right) (\mathbf{u} - \xi u \mathbf{n}). \end{aligned} \quad (14)$$

As it could be expected from symmetry considerations, $\mathbf{v}_1|_{x=\pm 1} = 0$ at $\xi = \pm 1$, i.e., at both poles. Note that result (14) validates the estimate $|\mathbf{v}_1| \sim (u^2/c^2) \max\{u, \nu R\}$ given above.

On the basis of velocity correction (14) and using Eq. (8), it is a straightforward matter to calculate a compressibility correction to the pressure $p_1 = p - p_0$. This is performed in Appendix B. It is worth mentioning that in the general case, correction to the pressure (B4) includes solely even powers of ξ , so that corresponding correction to an additional force exerted on the projectile due to dissipation in the surrounding particle fluid [Eq. (10) in Ref. [23]] vanishes. In the friction-dominated regime (large κ), one can retain in (B4) solely the term proportional to u^2 , which is independent of ξ , so that the total pressure is

$$p(\xi) \simeq p_{\text{st}} + \frac{\rho_0 u \nu R}{2} \xi + \frac{\rho_0 u^2}{8} \left(9\xi^2 - 5 + \frac{4\nu^2 R^2}{3c^2} \right). \quad (15)$$

Thus, the pressure increases due to finite compressibility, so that the threshold velocity of cavity deformation increases as well. On the other hand, one can see that the resulting correction is small when $\kappa u/c \ll 1$. However, we will see that the finite compressibility correction is always small for large projectiles even if this condition is not satisfied.

Now we repeat the analysis of Sec. II for Eq. (15) instead of (6). Since the finite compressibility correction is independent of ξ , the expression for ξ_{cr} remains the same as in Sec. II. Consider first the case $|\xi_{\text{cr}}| > 1$, when we have to set $\xi = -1$ in Eq. (15) to find the threshold velocity corresponding to emergence of a point of zero pressure at the ‘‘rear pole’’ of a cavity:

$$u_{\text{cr}} = \frac{\nu R}{2\omega} - \sqrt{\frac{\nu^2 R^2}{4\omega^2} - \frac{2p_{\text{st}}}{\omega\rho_0}} \simeq \frac{2p_{\text{st}}}{\nu R\rho_0}, \quad (16)$$

where $\omega = 1 + \nu^2 R^2/3c^2$. For the case of large cavities ($R \rightarrow \infty$) typical for treated case, approximation (16) is valid provided that the condition $p_{\text{st}}/\rho_0 c^2 \ll 1$, which applies to experiments analyzed in Sec. IV, is satisfied even if $\kappa u/c > 1$. Thus, finite compressibility seems to have no significant effect on the critical velocity. The reciprocal dependence $p_{\text{st}}(u_{\text{cr}})$ has the form

$$\frac{p_{\text{st}}}{\rho_0} = \frac{\omega u_{\text{cr}}^2}{2} \left(\frac{\nu R}{\omega u_{\text{cr}}} - 1 \right) \simeq \frac{1}{2} \nu R u_{\text{cr}}. \quad (17)$$

Upon further increase of the projectile velocity u , the region of negative pressure on the surface of a cavity is expanded. It is a straightforward matter to demonstrate that extrapolation of the theory to the extended region of negative pressures (where it is formally invalid) results in a very fast increase of this region with the increase of u . Therefore, u_{cr} is likely to be a good estimate for the stall velocity u_{st} . At the same time, $u_{\text{st}} > u_{\text{cr}}$ means that if we equate $u_{\text{cr}} = u_{\text{st}}$ we obtain from (17) an overestimated

p_{st} , which can be treated as an *upper bound estimate* for the static pressure.

In the case $|\xi_{\text{cr}}| < 1$ typical for small projectiles, a circle with zero pressure first emerges at the critical velocity

$$u_{\text{cr}} = 2 \left(\frac{2p_{\text{st}}}{5\rho_0} - \frac{\nu^2 R^2}{45} \right)^{1/2} \left(1 - \frac{4\nu^2 R^2}{15c^2} \right)^{-1/2} \simeq \left(\frac{8p_{\text{st}}}{5\rho_0} \right)^{1/2}. \quad (18)$$

Here, the approximation corresponding to the limit $R \rightarrow 0$ also coincides with that for an incompressible fluid. If u_{cr} is known from experiment, one can derive an upper bound estimate for the static pressure,

$$\frac{p_{\text{st}}}{\rho_0} = \frac{5u_{\text{cr}}^2}{8} + \frac{\nu^2 R^2}{18} \left(1 - \frac{3u_{\text{cr}}^2}{c^2} \right) \simeq \frac{5u_{\text{cr}}^2}{8}. \quad (19)$$

In this case at $u > u_{\text{cr}}$, the circle expands to a region between two circles on the surface of a cavity. For small projectiles, one can also demonstrate that a fast expansion of the negative region takes place as u is increased. Thus, u_{cr} also yields a reasonable order of magnitude estimate for a stall threshold.

IV. COMPARISON WITH EXPERIMENT

Based on developed theory we will analyze the possibility of cavity deformation in experiments. Consider first the experiments carried out in the PK-3 Plus Laboratory onboard the ISS under microgravity conditions. Details on the setup can be found in [18]. Dust particles injected into the main plasma with dispensers formed a cloud around the center of the chamber. Some larger particles present in the chamber as well get sporadically accelerated and penetrate into the cloud, thus forming projectiles [25]. Consider the experiment with argon as a carrier gas. For a gas pressure and temperature of 10 Pa and $T_n = 300$ K, respectively, we have $m_n = 6.63 \times 10^{-23}$ g, $n_n = 2.42 \times 10^{15}$ cm $^{-3}$, and $v_{T_n} = 2.5 \times 10^4$ cm/s. A dust cloud was formed by melamine-formaldehyde particles with the radius $a_d = 1.275 \times 10^{-4}$ cm and mass $M_d = 1.31 \times 10^{-11}$ g [19, 22], therefore, $\nu = 46.6$ s $^{-1}$.

Successive frames of the path of a projectile recorded by a high-resolution camera are shown in Fig. 2. The projectile velocity increases slowly from $u = 0.7$ cm/s to 1.4 cm/s. Since the sound velocity measured in this experiment amounts to 2.2 cm/s [19], such motion is subsonic. The peculiarity of this motion is an abrupt change of cavity configuration. At the beginning, the projectile moves in the center of a cavity [cf. Figs. 2(a) and (b)]. Then, at the point of trajectory characterized by the velocity $u = 1.06$ cm/s, acceleration $\dot{u} = 2.6$ cm/s 2 , and the cavity radius $R = 3.74 \times 10^{-2}$ cm, the projectile shifts abruptly from the cavity center to its front side [Fig. 2(c)]. In the course of further motion, cavity deformation is preserved [Fig. 2(d)]. One can assume that at

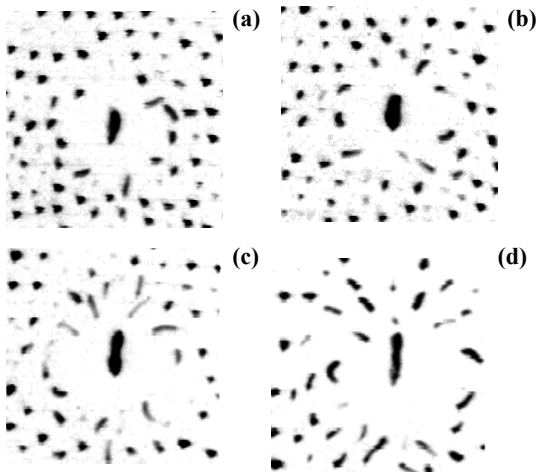


FIG. 2. Positions of dust particles and the projectile (negative images) at successive instants. Time interval between individual frames is 0.08 s. Frames (a) and (b) illustrate a spherical cavity; (c) and (d), deformed cavity. The projectile is accelerated from (a) to (d).

the point shown in Fig. 2(c), the velocity of the accelerating projectile exceeds a stall threshold. Under specified experimental conditions, $\xi_{\text{cr}} = -0.365$, hence we substitute $u_{\text{cr}} = 1.06$ cm/s in (19) to derive an upper bound estimate $p_{\text{st}}/\rho_0 \approx 0.753$ cm²/s² (or $p_{\text{st}} \approx 3.0 \times 10^{-7}$ Pa). Note that the correction for acceleration to the total pressure $-\rho\dot{u}R/2$ [Eq. (6)] is small due to a small projectile acceleration at selected point ($\dot{u}/u \ll \nu$) and can be neglected.

The estimate obtained above can be compared with a theoretical estimation for the static pressure, which is based on dimensionality considerations. Since dimensionalities of the pressure and energy density coincide, we can write with an order of magnitude accuracy $p_{\text{st}} \sim Z_d^2 e^2 n_d / 2\bar{r}$, where $\bar{r} = (3/4\pi n_d)^{1/3}$ is the Wigner-Seitz radius for a dust crystal and n_d is the number density of dust particles. With $Z_d = 1200$ and $n_d = 3 \times 10^5$ cm⁻³ [19], this estimation yields $p_{\text{st}} \sim 5.4 \times 10^{-7}$ Pa, which correlates with the upper bound estimate resulting from experiment.

Microgravity conditions can also be maintained on parabolic flights. Such experiments were performed using the IMPF-K2 chamber [11]. The experiment was carried out with argon at 30 Pa and $a_d = 4.775 \times 10^{-4}$ cm ($M_d = 6.88 \times 10^{-10}$ g and $\nu = 33.5$ s⁻¹). Projectiles were accelerated by a special device (cogwheel) up to both supersonic and subsonic velocities. A typical image illustrating the motion of a subsonic projectile inside a dust cloud is shown in Fig. 3. Both the projectile shift from the cavity center toward its front side and the nonspherical (elongated) shape of a cavity are visible. Unfortunately, a point of transition from a spherical to a deformed cavity was not detected in this experiment. Nevertheless, we can estimate the stall threshold for this case. Note that here, the estimate $p_{\text{st}} \sim Z_d^2 e^2 n_d / 2\bar{r}$

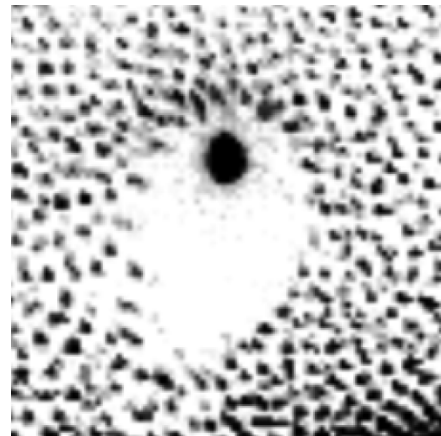


FIG. 3. Deformed cavity around a large subsonic projectile moving with the velocity $u = 1.8$ cm/s. Reproduction of an enlarged fragment of Fig. 3a in Ref. [11].

with $Z_d = 8800$ and $n_d = 2 \times 10^4$ cm⁻³ [11] yields $p_{\text{st}} \sim 7.8 \times 10^{-7}$ Pa, which is close to the estimate for experiment [22] discussed above. Therefore, we can assume that p_{st} are close in both systems and use the upper bound estimate (16) to calculate u_{cr} for the treated system. With the cavity radius roughly estimated as $R = 0.1$ cm, we derive $u_{\text{cr}} \approx 0.462$ cm/s, so that the projectile moves in the low-velocity regime ($\xi_{\text{cr}} = -1.61$). Therefore, the stall threshold for this system does not exceed 1 cm/s. This result correlates with the projectile velocity in Fig. 3, $u = 1.8$ cm/s, which is still lower than the sound velocity $c = 2.0$ cm/s [11]. Thus, the main notion of the present study, namely that the cavity around a moving projectile can be deformed at *subsonic velocity*, is corroborated.

V. CONCLUSION

We have investigated the possibility of the deformation of a cavity around large projectiles slowly moving inside a cloud of small dust particles. This cavity is formed due to a strong Coulomb repulsion between the projectile and dust particles. Since the parameter β_{dp} characterizing this interaction is very large, cavity deformation occurs solely due to the formation of a void adjacent to the initially spherical cavity. This is similar to the process of void formation in a fluid under negative pressure. Since we approximate the dust cloud by a system of hard spheres, zero pressure is sufficient for void formation leading to cavity deformation.

We model a collective particle subsonic motion in a complex plasma by nonviscous irrotational hydrodynamic motion of dust fluid and show that, in this model, the reason for cavity deformation is the friction between dust particles and neutral atoms of a carrier gas. It is this friction that stipulates the emergence of a zone of nega-

tive pressure over the back of a cavity surface. If such a zone covers a substantial part of the surface, stall takes place, which is observed as cavity deformation. We have found that the deformation is more likely to be observed for larger projectiles. The deformation occurs when the projectile velocity exceeds some threshold of subsonic velocity.

Since typical projectile velocities are of the same order of magnitude as the sound velocity, we have studied the effect of finite compressibility of the dust fluid on velocity and pressure fields. Toward that end, we have obtained an exact solution of linearized gas dynamics equations for compressible nonviscous fluid flowing about the cavity. In so doing, we included both the convective and friction terms in the Navier–Stokes equation. Calculations showed that corrections for finite compressibility are rather small. Generally, account of the compressibility leads to a shift of the area covered by a negative pressure zone.

Analysis of available experimental data has validated our approach. It was found that the cavity is deformed when either the velocity [22] or the size [11] of a projectile is sufficiently large. It is worth mentioning that the phenomenon of cavity deformation is similar to the formation of a void behind a cluster of smaller particles moving in the cloud of larger ones [26]. For intermediate projectile sizes, a transition from a spherical to a deformed cavity was observed along the trajectory of an individual projectile. The transition threshold is in accordance with the developed theory. This made it possible to estimate the static pressure inside a dust cloud and, hence, opened up a possibility to use projectiles as a diagnostic tool for the dust equation of state.

In this study, we restricted ourselves to an investigation of the threshold of cavity deformation and did not address the shape of the deformed cavity or displacement of the projectile away from the center of its cavity. This problem would require an adequate account of the local nonspherical charge distribution around the projectile. It is also possible that the observed shift of the projectile from the center of a cavity is noticeably favored by an additional drag force exerted on the projectile [23].

Appendix A:

The solution of Eq. (12) with boundary conditions (13) is represented in the form

$$\tilde{\varphi}_1(x, \xi) = \sum_{l=0}^3 f_l(x) P_l(\xi), \quad (\text{A1})$$

where $f_l(x)$ are the coefficients of expansion in the Legendre polynomials $P_l(\xi)$. We substitute (A1) in (12) taking into account that $\nabla^2 P_l(\xi) = -l(l+1)x^{-2}P_l(\xi)$ to reduce Eq. (12) to a set of ordinary differential equations

in spherical coordinates for nonzero functions $f_l(x)$,

$$\frac{d}{dx} \left(x^2 \frac{df_l}{dx} \right) - l(l+1)f_l = q_l(x), \quad (\text{A2})$$

where $q_0(x) = \frac{1}{2}\kappa x^{-4}$, $q_1(x) = \frac{36}{5}x^{-5} - \frac{9}{2}x^{-8}$, $q_2(x) = -\kappa x^{-1} + \frac{1}{2}\kappa x^{-4}$, $q_3(x) = -6x^{-2} + \frac{24}{5}x^{-5} - \frac{3}{2}x^{-8}$. The boundary conditions for (A2) follow from (13):

$$f_l(\infty) = 0, \quad \left. \frac{df_l}{dx} \right|_{x=1} = 0. \quad (\text{A3})$$

The rhs of (A2) has the form $\sum_k b_{lk} x^{-k}$, where b_{lk} are constants entering the functions $q_l(x)$. Solution of (A2) is then given by

$$f_l(x) = \frac{C}{x^{l+1}} + \sum_k \frac{b_{lk}}{k(k-1) - l(l+1)} \frac{1}{x^k}, \quad (\text{A4})$$

where C is defined by the second boundary condition (A3), whence it follows that

$$f_l(x) = \sum_k \frac{b_{lk}}{l(l+1) - k(k-1)} \left(\frac{k}{l+1} \frac{1}{x^{l+1}} - \frac{1}{x^k} \right). \quad (\text{A5})$$

Finally, we obtain

$$f_0 = \kappa \left(-\frac{1}{6x} + \frac{1}{24x^4} \right), \quad (\text{A6})$$

$$f_1 = -\frac{2}{3x^2} + \frac{2}{5x^5} - \frac{1}{12x^8}, \quad (\text{A7})$$

$$f_2 = \kappa \left(\frac{1}{6x} - \frac{1}{6x^3} + \frac{1}{12x^4} \right), \quad (\text{A8})$$

$$f_3 = \frac{3}{5x^2} - \frac{54}{55x^4} + \frac{3}{5x^5} - \frac{3}{88x^8}. \quad (\text{A9})$$

$$(\text{A10})$$

Appendix B:

The pressure correction due to finite compressibility can be found using the corresponding velocity correction, Eq. (14). We rewrite Eq. (8) in the form

$$-c^2 \nabla \ln \rho = \frac{1}{2} \nabla v^2 + \nu \nabla \varphi, \quad (\text{B1})$$

where $\varphi = \varphi_0 + \varphi_1$ and $\mathbf{v} = \mathbf{u} + \nabla \varphi$. By integrating Eq. (B1) we derive

$$\begin{aligned} \rho - \rho_0 = & -\frac{\rho_0}{c^2} \left(\frac{v_0^2}{2} + \nu \varphi_0 \right) - \frac{\rho_0}{c^2} (\mathbf{v}_0 \cdot \mathbf{v}_1 + \nu \varphi_1) \\ & + \frac{\rho_0}{2c^4} \left(\frac{v_0^2}{2} + \nu \varphi_0 \right)^2, \quad (\text{B2}) \end{aligned}$$

where $\rho_0 = \rho|_{r=\infty}$ and the terms up to $(u/c)^4$ are retained (for simplicity we assume $c = \text{const}$). We write

the equation of state for the dust fluid in the form $p - p_{\text{st}} = c^2(\rho - \rho_0)$, which yields

$$p = p_{\text{st}} - \frac{\rho_0 v_0^2}{2} - \nu \rho_0 \varphi_0 - \rho_0 \mathbf{v}_0 \cdot \mathbf{v}_1 - \nu \rho_0 \varphi_1 + \frac{1}{2\rho_0 c^2} \left(\frac{\rho_0 v_0^2}{2} + \nu \rho_0 \varphi_0 \right)^2. \quad (\text{B3})$$

The first three terms of Eq. (B3) represent Eq. (6) with $\dot{u} = 0$. Hence, by substituting in Eq. (B3) the expressions

for φ_0 and \mathbf{v}_0 [Eqs. (4) and (5)] as well as for φ_1 and \mathbf{v}_1 [Eq. (14)] taken at the cavity surface, we get

$$p_1(\xi) = \frac{\rho_0 u^4}{c^2} \left[\frac{1}{6} \kappa^2 - 3\kappa \xi^2 \left(\xi^2 - \frac{101}{440} \right) - \frac{2025}{1408} \left(\xi^4 - \frac{5414}{3375} \xi^2 + \frac{5237}{10125} \right) \right]. \quad (\text{B4})$$

-
- [1] V. E. Fortov and G. E. Morfill, eds., *Complex and Dusty Plasmas: From Laboratory to Space*, Series in Plasma Physics (CRC Press, 2009).
- [2] J. H. Chu and L. I, Phys. Rev. Lett. **72**, 4009 (1994).
- [3] H. Thomas, G. E. Morfill, V. Demmel, J. Goree, B. Feuerbacher, and D. Möhlmann, Phys. Rev. Lett. **73**, 652 (1994).
- [4] Y. Hayashi and S. Tashibana, Jpn. J. Appl. Phys. **33**, L804 (1994).
- [5] S. V. Vladimirov, K. Ostrikov, and A. A. Samarian, *Physics and applications of complex plasmas* (Imperial College, London, 2005).
- [6] V. Fortov, A. Ivlev, S. Khrapak, A. Khrapak, and G. Morfill, Phys. Rep. **421**, 1 (2005).
- [7] G. E. Morfill and A. V. Ivlev, Rev. Mod. Phys. **81**, 1353 (2009).
- [8] P. K. Shukla and B. Eliasson, Rev. Mod. Phys. **81**, 25 (2009).
- [9] M. Bonitz, C. Henning, and D. Block, Rep. Prog. Phys. **73**, 066501 (2010).
- [10] G. E. Morfill, U. Konopka, M. Kretschmer, M. Rubin-Zuzic, H. M. Thomas, S. K. Zhdanov, and V. Tsytovich, New J. Phys. **8**, 7 (2006).
- [11] D. Caliebe, O. Arp, and A. Piel, Phys. of Plasmas **18**, 073702 (2011).
- [12] A. Piel, O. Arp, M. Klindworth, and A. Melzer, Phys. Rev. E **77**, 026407 (2008).
- [13] K. O. Menzel, O. Arp, and A. Piel, Phys. Rev. E **83**, 016402 (2011).
- [14] O. Arp, D. Caliebe, and A. Piel, Phys. Rev. E **83**, 066404 (2011).
- [15] M. Schwabe, S. K. Zhdanov, H. M. Thomas, A. V. Ivlev, M. Rubin-Zuzic, G. E. Morfill, V. I. Molotkov, A. M. Lipaev, V. E. Fortov, and T. Reiter, New J. Phys. **10**, 033037 (2008).
- [16] G. E. Morfill, H. M. Thomas, U. Konopka, H. Rothermel, M. Zuzic, A. Ivlev, and J. Goree, Phys. Rev. Lett. **83**, 1598 (1999).
- [17] S. A. Khrapak, B. A. Klumov, P. Huber, V. I. Molotkov, A. M. Lipaev, V. N. Naumkin, H. M. Thomas, A. V. Ivlev, G. E. Morfill, O. F. Petrov, V. E. Fortov, Y. Malentschenko, and S. Volkov, Phys. Rev. Lett. **106**, 205001 (2011).
- [18] H. M. Thomas, G. E. Morfill, V. E. Fortov, A. V. Ivlev, V. I. Molotkov, A. M. Lipaev, T. Hagl, H. Rothermel, S. A. Khrapak, R. K. Suetterlin, M. Rubin-Zuzic, O. F. Petrov, V. I. Tokarev, and S. K. Krikalev, New J. Phys. **10**, 033036 (2008).
- [19] M. Schwabe, K. Jiang, S. Zhdanov, T. Hagl, P. Huber, A. V. Ivlev, A. M. Lipaev, V. I. Molotkov, V. N. Naumkin, K. R. Sütterlin, H. M. Thomas, V. E. Fortov, G. E. Morfill, A. Skvortsov, and S. Volkov, EPL **96**, 55001 (2011).
- [20] M.-C. Chang, Y.-P. Tseng, and L. I, Phys. of Plasmas **18**, 033704 (2011).
- [21] D. Samsonov, J. Goree, H. M. Thomas, and G. E. Morfill, Phys. Rev. E **61**, 5557 (2000).
- [22] D. I. Zhukhovitskii, V. E. Fortov, V. I. Molotkov, A. M. Lipaev, V. N. Naumkin, H. M. Thomas, A. V. Ivlev, M. Schwabe, and G. E. Morfill, Phys. Rev. E **86**, 016401 (2012).
- [23] A. V. Ivlev and D. I. Zhukhovitskii, Phys. Plasmas **19**, 093703 (2012).
- [24] L. D. Landau and E. M. Lifshitz, *Fluid Mechanics* (Pergamon Press, New York, 1959).
- [25] J. Goree, G. E. Morfill, V. N. Tsytovich, and S. V. Vladimirov, Phys. Rev. E **59**, 7055 (1999).
- [26] K. R. Sütterlin, A. Wysocki, A. V. Ivlev, C. R. R. Räth, H. M. Thomas, M. Rubin-Zuzic, W. J. Goedheer, V. E. Fortov, A. M. Lipaev, V. I. Molotkov, O. F. Petrov, G. E. Morfill, and H. Löwen, Phys. Rev. Lett. **102**, 085003 (2009).